J Exp Biol Advance Online Articles. First posted online on 13 March 2014 as doi:10.1242/jeb.098046
Access the most recent version at http://jeb.biologists.org/lookup/doi/10.1242/jeb.098046

Undulatory locomotion of flexible foils as biomimetic models for understanding fish propulsion

Ryan M. Shelton[1, 2], Patrick Thornycroft[1], and George V. Lauder[1]

[1] The Museum of Comparative Zoology, 26 Oxford St., Harvard University, Cambridge, MA 02138, USA

[2] Current address: Department of Biology, CB# 3280 Coker Hall, University of North Carolina Chapel Hill, NC 27599-3280

Author for correspondence:
George V. Lauder
E-mail: glauder@oeb.harvard.edu
Phone: 617-496-7199

Running title: Biomimetic models of fish locomotion

SUMMARY

An undulatory pattern of body bending in which waves pass along the body from head to tail is a major mechanism of creating thrust in many fish species during steady locomotion. Analyses of live fish swimming have provided the foundation of our current understanding of undulatory locomotion, but our inability to experimentally manipulate key variables such as body length, flexural stiffness, and tailbeat frequency in freely-swimming fish has limited our ability to investigate a number of important features of undulatory propulsion. In this paper we use a mechanical flapping apparatus to create an undulatory wave in swimming flexible foils driven with a heave motion at their leading edge, and compare this motion to body bending patterns of bluegill sunfish (*Lepomis macrochirus*) and clown knifefish (*Notopterus chitala*). We found similar swimming speeds, Reynolds and Strouhal numbers, and patterns of curvature and shape between these fish and foils suggesting that flexible foils provide a useful model for understanding fish undulatory locomotion. We swam foils with different lengths, stiffnesses, and heave frequencies while measuring forces, torques, and hydrodynamics. From measured forces and torques we calculated thrust and power coefficients, work, and cost of transport for each foil. We found that increasing frequency and stiffness produced faster swimming speeds and more thrust. Increasing length had minimal impact on swimming speed, but had a large impact on Strouhal number, thrust coefficient, and cost of transport. Foils that were both stiff and long had the lowest cost of transport (in mJ m^{-1} g^{-1}) at low cycle frequencies, and the ability to reach the highest speed at high cycle frequencies.

INTRODUCTION

Fish perform undulatory locomotion with their flexible bodies to move forward steadily by passing a wave of bending from the head toward the tail (Jayne and Lauder, 1995a; Lauder and Tytell, 2006; Long et al., 1994; McHenry et al., 1995). Undulatory propulsion involves sequential activation of the segmental musculature by the nervous system, and this wave of electrical activity passes back toward the tail at a higher speed than the wave of bending (Jayne and Lauder, 1995b, c; Rome et al., 1993; Syme and Shadwick, 2002). Kinematic studies have shown that in many fishes swimming steadily by undulatory propulsion, the front third of the body remains relatively still at lower swimming speeds, and as speed increases oscillations of the front portion of the body also increase heaving from side to side (review in Lauder and Tytell, 2006). The side-to-side (heave) motion of the body region increases in amplitude as it passes down the body (Long et al., 1994; Donley and Dickson, 2000). Analyses of tail (caudal fin) motion have also emphasized the role that this structure plays in generating propulsive forces (e.g., Affleck, 1950; Gibb et al., 1999; Magnuson, 1978), and three-dimensional body geometry clearly plays an important role in patterns of thrust generation (Tytell, 2006; Tytell et al., 2008).

These experimental studies of freely-swimming fishes have provided a wealth of information about the locomotion of a diversity of fish species, and have served to focus attention on different modes of fish propulsion and changes in locomotor style with environment (e.g., Liao et al., 2003a, b; Webb, 2006). But study of live fishes has certain limitations that cannot easily be overcome. For example, measuring the effects of changing flexural stiffness, cycle frequency, and body length cannot be isolated from the many other variables involved with a live swimming fish. Measuring forces on freely swimming fishes is also difficult (e.g., Peng et al., 2007, 2008). It is not possible to alter individual factors involved in undulatory propulsive dynamics and assess their contribution to swimming performance by studying live fishes alone.

However, simple robotic models of undulatory locomotion in fishes can be used to good advantage and allow relatively rapid alteration of experimental parameters, assessment of the effect of making these alterations on locomotor performance, and a comprehensive assessment of locomotor forces, torques, and derived physical quantities such as the cost of transport (Bhalla et al., 2013; Lauder et al., 2007, 2011a, 2012; Ramananarivo et al., 2013; Wen and Lauder, 2013). More complex robotic models of undulatory locomotion have the advantage of being more biomimetic (Barrett et al., 1999; Liu and Hu, 2006; Long et al.,

2006a, b, 2011; Tangorra et al., 2010), but are more difficult to alter quickly and change individual parameters like flexural stiffness.

In this paper we compare undulatory locomotion in two species of live fishes to swimming by four rectangular flexible foils driven by a robotic controller at their leading edge. The flexural stiffness of these two foils was chosen to match the passive body stiffness reported for fishes in the literature (Long et al., 1994, 2002). We analyze the self-propelled swimming speeds of these foils as we vary flexural stiffness, cycle frequency, and length. These three parameters were chosen because they encompass much of the variation in fish swimming kinematics based on previous studies of live fish locomotion (e.g., Bainbridge, 1958; Donley and Dickson, 2000; Webb, 1975), and because prior studies of swimming flexible foils suggested that length and stiffness were key parameters governing locomotor dynamics (Alben et al, 2012; Hua et al., 2013; Long et al., 1994). Although swimming foils of rectangular shape represent a considerable simplification of the complex three-dimensional geometries of fishes and ignore features such as tail structure, we focus here on the stiffness and length properties of swimming foils compared to fishes (maintaining uniform thickness and flexibility along the length), and future studies could extend the approach taken in this paper to more complex and fish-like flexible surfaces.

In this paper we compare undulatory foil swimming to that of live fish by measuring body curvature, swimming speed, cycle frequency, Strouhal number, and Reynolds number. Analysis of patterns of foil force and torque produced during swimming allows calculation of cost of transport, and force and power coefficients of these foils during self-propulsion. We initially hypothesized that, for the foils, swimming speed would increase with frequency based on previous data from swimming fishes (e.g., Bainbridge, 1958), that increasing length should reduce swimming efficiency due to the greater drag incurred by the longer foils actuated only at their leading edge, and that increasing stiffness (within the range studied here) would increase swimming efficiency and reduce cost of transport based on a previous study with foils of different shapes (Lauder et al., 2011b).

Our overall goal is to provide an analysis of the effects of length and flexural stiffness during steady swimming with undulatory waves using a mechanical flapping foil apparatus which allows exploration of the basic mechanics of undulatory propulsion in ways not possible by studying live fish, while recognizing that these swimming foils represent a considerable simplification of fish body geometry (Tytell et al., 2008). Finally, we suggest that this approach allows a general estimate of the flexural stiffness of the bodies of freely-swimming fishes, as measuring this parameter has to date been extremely challenging.

RESULTS

Foil and fish self-propelled kinematics

In both bluegill and clown knifefish, the front portion of the body moved much less than the posterior region throughout the tail beat cycle, and a wave of body bending passed from head toward the tail. Knifefish started undulatory motion halfway down the body (Fig. 1a) and created approximately three quarters of a wave along the body as seen in the expanded ventral view midline snapshots (Fig. 1c, e). Bluegill undulated with the last quarter of the body (Fig. 1b) and made roughly one quarter of a wave with reduced body bending compared to knifefish (Fig. 1d, f). The shape of the knifefish posterior body region during swimming (Fig. 1e) was very similar to the swimming shape of the tan 10 cm length flexible foil when actuated at 2 Hz (Fig. 2). Undulation of the sunfish posterior body region (Fig. 1f) resembled the stiffer yellow 10 cm foil actuated at 2 Hz (Fig. 2).

The effect of varying lengths, stiffness, and frequencies on foil swimming shape can be seen in Figure 2. Flexible tan foils had shorter wavelengths and larger amplitudes than the stiffer yellow foils. The longer foils had similar shapes and wavelengths to their shorter counterparts but continued the pattern over their longer length. Generating foil motion at higher frequencies increased the number of waves seen on each foil. The tan 20 cm foil showed an increase from 0.5 waves to 1.25 waves, and the yellow 20 cm foil increased from 0.25 waves to 0.6 waves over the frequency range of 0.5 to 3 Hz (Fig. 2).

Swimming speeds of bluegill and knifefish varied with cycle frequency, and the pattern of swimming speed change with frequency was similar to that observed in the two swimming foils (Fig. 3). Bluegill data points fall within the yellow foil data range, while knifefish data are at or just below tan foil velocities. Self-propelled speeds ranged from 7 to 14 cm s^{-1} at 1 Hz, 16 and 27 cm s^{-1} at 2 Hz, and 27 to 32 cm s^{-1} at 3 Hz for the foils and fish combined. The regression lines of fish and foils were similar in slope, although the tan foils had slightly lower slopes (Table 1). The coefficient of determination (R^2) showed a significant correlation between self-propelled speed and cycle frequency for all of the foils and knifefish, with a lower (but still significant) correlation for bluegill. Bluegill use their pectoral fins periodically even during undulatory swimming which may have caused greater variation in these data, even though sequences with minimal pectoral fin movement were chosen (also see Drucker and Lauder 2000, 2005).

Analysis of covariance (ANCOVA; also see Table 1) demonstrated (1) a highly significant effect of frequency (regression model $P<0.001$) for both fish and foils on swimming speed, (2) no significant difference between the fish and flexible tan foil regressions ($P> 0.06$), (3) no significant interaction between fish and flexible tan foil data ($P>0.7$), and (4) a significantly higher slope for the stiffer (yellow) foil regressions ($P<0.001$).

Measurement of maximum curvature for swimming fish or foils during a flapping cycle (Fig. 4) showed that foil curvatures for the stiff (yellow) foils remained small over the range of frequencies, while the more flexible tan foil curvatures increased steadily as frequency increased. This pattern is also visually evident in the foil midline snapshots shown in Figure 2. Foil length had little impact on maximum curvature. Curvature of the bluegill sunfish body was intermediate between the tan and yellow foil data at higher frequencies, while knifefish maximum body curvatures were higher than that of either foil (even excluding the very high curvature near the tail tip).

Reynolds numbers measured for swimming fish and self-propelling foils in this study were similar (Fig. 5a). Between 1 and 3 Hz, the frequencies for which we have data for both fish and foils (Fig. 5), fish Reynolds numbers ranged from 19,000 to 58,000 and foil Reynolds numbers ranged from 10,000 to 64,000. Over the same frequencies, fish Strouhal numbers measured here varied from 0.29 to 0.5 compared to foils with a range of 0.24 to 0.38 (Fig. 5b).

Foil swimming performance surfaces

Performance surfaces for short 10 cm (Fig. 6) and long 20 cm (Fig. 7) foils show that both thrust and efficiency tend to increase as frequency increases. The stiff (yellow) foils have higher thrust coefficients than flexible (tan) foils at both lengths although the difference in thrust is small at the highest frequencies at the slowest swimming speeds. For a given stiffness at most swimming speeds, the shorter 10 cm long foils generate higher thrust than the longer 20 cm foils. For example, at a swimming speed of 0.2 m/s, the stiff 10 cm foil produces a mean thrust coefficient nearly twice that of the 20 cm foil.

Swimming efficiency shows a more complex pattern. At the two highest swimming speeds at higher heave values, the stiff foils have greater locomotor efficiency (Figs. 6, 7) than the flexible foils. But at low swimming speeds the flexible tan foils have generally higher efficiencies. For example, at a swimming speed of 0.1 m/s, the 10 cm long flexible foil has higher swimming efficiency for most of the frequency range (Fig. 6). At this same swimming speed, the 20 cm long foil curves cross so that below 1.6 Hz (Fig. 7), the stiff foil

has greater efficiency while above this frequency the flexible foil has equal or greater efficiency. In general, as swimming speed increases, the disparity in efficiency between stiff and flexible foils increases, so that at the highest swimming speed of 0.3 m/s the stiff foils of both lengths show substantially greater efficiency than the flexible foils.

Foil dynamics during self-propulsion

When swimming foils are self-propelling, the thrust (Fx) and heave forces (Fy) sum to zero when averaged over a flapping cycle. Therefore, force and torque ranges within a flapping cycle were measured to compare the magnitude of oscillation over a cycle. Repeated force measurements to assess error showed that one standard error of the mean for force and torque measurements ranged from 0.4% of the mean to 1.0% of the mean, and error bars are not shown in Figure 5 as they fall within the symbols. Yellow (stiffer) foils produced a significantly higher Fx range at middle frequencies (e.g., 2 Hz, Fig. 5c), and a higher Fy range at the two higher frequencies (Fig. 5d). At the lowest frequencies of 0.5 and 1.0 Hz, stiffness had relatively little effect on either Fx or Fy oscillation magnitudes. The ratio of Fy to Fx varied from 4.4 to 29.4 with a mean of 15.1, indicating that the output thrust forces were approximately 7% of input heave force. The torque from the twisting of the foil during swimming (Tz) was minimal for the tan foils with a maximum range of 4.3 N mm, and was substantially larger for yellow foils at the two highest frequencies with a maximum range of 29.0 N mm (Fig. 5e). All of the forces and torques increased as frequency increased. Foil length had a relatively small effect on forces and torques.

The work done by each foil per cycle (Fig. 5f) increased with frequency and foil stiffness, while foil length made little difference. The cost of transport with respect to distance showed that being stiffer, and operating at higher frequencies took more energy (Fig. 5g), while foil length had only a small effect on cost. When standardized to foil mass, however, shorter, more flexible foils at higher frequencies require significantly more energy to swim at a given speed than other foils (Fig. 5h).

Over one flapping cycle, Fx (Fig. 8a) varied at twice the heave frequency, while Fy varied at the heave frequency (Fig. 8b), and no phase shifts in peak thrust were observed between foils of different lengths or stiffnesses. Thrust coefficients had a mean of zero over a flapping cycle as is expected for self-propelling foils. Shorter foils had approximately double the maximum thrust coefficient (of approximately 0.2) compared to the longer foils (Fig. 8c). Long foils had a maximum power coefficient of 0.6 while the short foils had a

maximum of 1.2 (Fig. 8d). From 1 to 3 Hz the mean power coefficients ranged from 0.23 to 0.73.

Foil hydrodynamics

The minimum absolute streamwise force (Fx) on the tan 10 cm (Fig. 9a) and yellow 10 cm (Fig. 9b) foils occurred just prior to the foil shaft reaching its maximum lateral excursion when heave speed is slowing and a vortex is shed from the trailing edge of both foils. Maximum streamwise force (Fig. 9c, d) occurred just prior to the shaft reaching its midpoint with maximum heave speed, and when a large leading edge vortex formed at the upstream foil margin for both foils. This x-force maximum occurred once while the foil was heaving to one side, and once while heaving to the other side, causing the x-force to oscillate with twice the heave frequency. Heave force (Fy) oscillated with heave motion and peak Fy displayed a 17% phase shift relative to heave motion for both the tan 10 cm and yellow 10 cm foils. This same pattern was observed for all foils at all frequencies. The mean Fx phase shift for all foils relative to heave motion was -3.9%.

DISCUSSION

Comparisons between fish and foils

Freely-swimming fish and passively flexible foils driven only at the leading edge have remarkably similar patterns of curvature and shape, Strouhal and Reynolds numbers, and changes in swimming speed with frequency (Figs. 1-3). However, ANCOVA analysis showed that the stiffer foils have increased slopes relative to both the more flexible tan foils and fish data, which collectively are not significantly different from each other (Table 1).

Although at first it might seem surprising that we should find such similarities, there are at least four reasons to expect that the locomotor performance of flexible foils and fish might be generally similar. First, when fish swim at speeds less than about two body lengths per second, only red muscle fibers are activated, and the large mass of white fibers in the body musculature is inactive electrically. In some fish such as largemouth bass (Jayne and Lauder, 1995b; Johnson et al., 1994) the red fibers only constitute about 1.5% of the body musculature, and during normal undulatory locomotion these fibers are thus bending a largely passive body in a flapping motion. Red muscle fibers are located in a thin strip down the midline of each side of the body just under the skin of most fishes. Patterns of body bending and hydrodynamics are thus dominated by properties of the mostly inactive body. White

muscle fibers which dominate the body mass are active only in high-speed (often unsteady) swimming motions, and during the c-start escape response of fishes (e.g., Jayne and Lauder, 1993, 1994, 1995b).

Second, when fish are self-propelling at slow to moderate speeds with the anterior half of the body undergoing minimal side-to-side (heave) oscillation (Lauder and Tytell, 2006), this body region is experiencing primarily drag force while the posterior body region is primarily generating thrust. At these swimming speeds, there is some spatial segregation of drag and thrust: when summed over the entire body, at self-propelled speeds net thrust must be equal and opposite to net drag. Regions of the locomotor performance space in which the swimming foils generate net thrust (Figs. 6, 7) are thus directly comparable to the thrust generating posterior body region. As a result, it is not surprising that kinematics of foils and the posterior region of self-propelling fish bodies are similar (Figs. 1, 2), and generate similar peak thrust forces of between 20 and 40 mN (Fig. 8) which is comparable to values estimated for mackerel swimming at one to two body lengths per second (Nauen and Lauder, 2002a).

Third, several important behaviors exhibited by fishes swimming in flows have been shown to involve a nearly completely passive body. For example, trout swimming in a vortex street are able to alter the amplitude of their tail beat and pattern of body bending to utilize the vortical energy to maintain position passively. This behavior, termed the Karman gait, has been observed in several species (Liao et al., 2003a, b; Liao, 2004). Study of flexible foils and freshly dead fish in a vortex street also demonstrated the ability of passive fish bodies to hold position and create thrust (Beal et al., 2006).

Fourth, an additional feature of this study is our use of two flexible foils that possess flexural stiffnesses that are roughly equivalent to values that have been measured for dead fishes. Quantifying the time dependent flexural stiffness of a freely-swimming fish is a difficult challenge that has yet to be successfully accomplished. But a number of studies have estimated the flexural stiffness of fresh fish bodies, and we can compare these values to those measured for the flexible tan and yellow foils studied here. Long et al. (2002) measured the stiffness of freshly dead hagfish bodies, *Myxine glutinosa*, at a value of 3×10^{-4} Nm^2. A separate study showed that when the muscles in freshly dead American eels, *Anguilla rostrata*, were activated with an electric current, the body flexural stiffness reached a value of triple the passive flexural stiffness, measured at 1.8×10^{-4} Nm^2 (Long, 1998). By comparing the swimming of live pumpkinseed sunfish (*Lepomis gibbosus*, closely related to and very similar in shape to the bluegill sunfish studied here), to the swimming of three-dimensional

vinyl models of sunfish, it was predicted that sunfish double their passive body stiffness while swimming (McHenry et al., 1995): values measured for passive sunfish bodies ranged from approximately 1×10^{-3} N m^2 near the head, to 1×10^{-6} N m^2 near the tail.

Based on the similar kinematics (Figs. 1 and 2) and similar self-propelled swimming speeds relative to cycle frequency (Fig. 3, Table 1) between swimming knifefish and the tan foils, we predict that live swimming knifefish have a flexural stiffness similar to that of the tan foil material ($3.3 * 10^{-5}$ N m^2). Furthermore, we expect that swimming sunfish have a similar body flexural stiffness to the yellow foil material ($9.9 * 10^{-4}$ N m^2). Using flexible foils of similar flexural stiffness to that estimated for fishes allows us to quantify dynamics such as patterns of forces and torques throughout the flapping cycle that would be impossible on a freely-swimming fish.

Although the kinematic patterns displayed by undulatory fish motion (Fig. 1) and the flexible foils studied here (Fig. 2) are generally similar, it is noteworthy that the flexible foils under self-propulsion tend to show only limited amplitude increases along their length compared to kinematic patterns typically shown by swimming fishes. This difference could be due to several factors, most importantly the uniform flexural stiffness of the foils compared to the complexly varying body stiffness of fishes, both temporally during a locomotor cycle, and also spatially along the body. But the swimming foils, under conditions of net thrust generation (i.e., the positive thrust coefficient region of the performance surfaces in Figures 6 and 7) do show amplitude increases along their length (data not shown here). This suggests that foils swimming under these conditions could be thought of as functioning like the posterior body region of swimming fishes, generating net thrust in distinction to the generally low amplitude drag-incurring anterior body region. Further comparisons of foil kinematics under different thrust conditions as well as the study of flexible foils with different stiffness properties along their length will help in explaining the cause of kinematic amplitude differences between fish and swimming foils.

Flexible foil propulsion

Analysis of foil propulsion data demonstrates that self-propelled swimming speeds, forces, and torques increase as frequency and foil stiffness increase, but that length increase makes relatively little difference in locomotor performance (Figs. 3, 6, 7). Overall, the work done per cycle ranges from 0.5 to 21.7 mJ, the cost of transport (COT) with respect to distance ranges from 3.2 to 204.6 mJ m^{-1}, and the cost of transport with respect to distance and mass together ranges from 2.0 to 106.6 mJ m^{-1} g^{-1}. The work per cycle and cost of transport with

respect to distance follows similar trends to the self-propelled speeds, but the cost of transport relative to mass and distance shows that stiffer and longer foils are more efficient when foils swim at their self-propelled speeds. Averaging all of the trials, 10 cm foils cost 80% more than 20 cm foils, and flexible tan foils cost 159% more than the stiffer yellow foils when COT is measured in mJ m^{-1} g^{-1}. This suggests that when comparing flexible propulsors of equal mass, the longer stiffer foils can swim more efficiently given the stiffness range studied here at self-propelled speed, and this is also reflected in the efficiency values shown in Figure 7 over a range of swimming speeds. The longer, stiff foil achieved higher efficiencies than the short flexible foil at higher swimming speeds. Stiffer propulsors, like the yellow foils, are also able to reach higher speeds when they expend more energy.

Lauder et al. (2011b) presented data on self-propelled swimming speeds of flexible foils of fixed length versus flexural stiffness that covers a greater range of flexural stiffness than that studied here. They showed that for foils actuated in heave only at the leading edge, an optimum flexural stiffness existed at which swimming speed was maximized. When pitch actuation was added to the heave motion, however, no single peak swimming speed was found, and instead a broad plateau at which stiffness had little effect on swimming speed occurs above a flexural stiffness of $0.2 * 10^{-4}$ N m^3. Although no forces were measured in the Lauder et al. (2011b) study, those data in conjunction with those presented here suggest that modulation of the motion program and stiffness can be used to alter swimming performance. If fish muscle activation patterns can be tuned to alter the motion of the flexible body, and body stiffness altered over a three-fold range by changing the activation of body or fin musculature, then fish may be able to adjust their position on the performance curve to suit the demands of any particular locomotor situation.

In this study we focused on comparisons between flexible foils of two lengths and found relatively few substantial effects of differences between the 10 cm and 20 cm length on self-propelled swimming speed, although length did affect the cost of transport calculations by changing the mass of the swimming foils. However, the effect of length alone on swimming performance can be complex, with the occurrence of resonance peaks at different lengths. Alben et al. (2012) describe an analytical model of foil swimming performance and demonstrate a resonance phenomenon whereby the swimming speed of flexible foils can change in a non-linear manner that depends on foil length and stiffness. They modeled locomotion over a wide range of foil lengths to illustrate how foil length can affect swimming speed and found that certain lengths can interact negatively with flows generated near the front of the foil, and that this slows down self-propelled swimming speeds. Other foil lengths

can induce positive interactions that result in faster swimming speeds. In this paper we only studied foils of two different lengths, and did not find any substantial differences in self-propelled swimming speeds between these two lengths for the two foil materials studied. But a more complete study of a wide variety of foil lengths may find effects on thrust and cost of transport that are were not detectable here with a study of only two lengths.

We are not aware of other studies that have measured forces and torques from self-propelling foils with fish-like flexibility, but it is useful to compare our mean power coefficients with those from stiff (inflexible) towed foils as represented by the experiments reported by Read et al. (2003). At a Strouhal number of 0.28, the mean from our foils, Read et al. measured mean power coefficients around 0.6 which is slightly higher than our mean of 0.43. Rigid foils should be able to produce more propulsive power than a highly flexible foil under certain conditions, but it is noteworthy that power coefficient values for these highly flexible foils are in the same general range as those for stiff foils. The instantaneous power coefficient drops below zero for a small fraction of the cycle for all of the foils that we studied, which means that at this moment the water was doing work on the foil, but this effect is greater for the flexible tan foil than for the stiffer yellow foil (Fig. 8). The peak to peak thrust coefficient amplitudes for the flexible foils studied here range from 0.1 to 0.8 which is much less than that observed for rigid foils where peak thrust coefficients can reach values of 2.

When foils are self-propelling, all of the mean thrust coefficients equal zero (averaged over a flapping cycle), and this is an important condition of true self-propulsion: data shown for foils in which the thrust coefficient does not average to zero over a cycle indicate that the foil was not self-propelling, but was being towed at a speed either higher or lower than self-propelled swimming speed -- see Lauder et al., 2011a. Data showing this pattern could also indicate that the thrust being generated by the towed flapping object or foil was not sufficient to overcome mean drag, and so the foil would not swim forward on its own if it were not being forcibly towed. However, given that the posterior region of the fish body is the region where muscular work is positive and contributing to thrust generation (Rome et al., 1993; Johnson et al., 1994), experimental conditions with a mean positive thrust coefficient (Figs. 6, 7) can be thought of as representing the thrust generating region of the fish body that must generate net positive thrust to overcome drag of the mostly immobile anterior body region.

Katz and Weihs (1979) conducted a computational study of a flexible slender wing and examined the effects of chordwise flexibility on thrust and efficiency of swimming. They found an increase in thrust coefficient up to an intermediate level of flexibility and a

plateau where little increase in thrust was seen as flexibility increased further. In our data,the stiff (yellow) foils showed higher thrust coefficients than the corresponding flexible (tan) foils of the same length. For foils of the same stiffness, shorter foils had higher thrust coefficients than the longer foils.

In this paper we show that flexible foils actuated only in heave at the leading edge perform in a manner generally similar to undulating fish bodies and we estimate that the flexural stiffness of two species of freely-swimming fishes is in the range of that measured for the foil materials that we studied here. However, future experiments could certainly expand on this approach to incorporate active flexion of body segments into the design of a flexible self-propelling model for fish propulsion. Past experiments on robotic devices of this nature have proven extremely useful in understanding the nature of locomotor dynamics in undulating bodies (e.g., Barrett et al., 1999). In addition, flexible foils could be used to study the dynamics of unsteady locomotor behaviors such as linear accelerations and c-start escape responses in fishes. These behaviors have received recent attention from experimental hydrodynamicists (Borazjani et al., 2012, Tytell, 2004, Tytell and Lauder, 2008) but have yet to be modeled with robotically controlled devices that allow direct measurement of forces and torques.

MATERIALS AND METHODS

We obtained data from two fish species, swimming freely in a recirculating flow tank, that differ in the pattern of body bending to permit comparison to similar data obtained for two robotic flapping foils that differ in flexural stiffness. We chose bluegill sunfish (*Lepomis macrochirus*, Rafinesque) and clown knifefish (*Notopterus chitala*, Hamilton) because they vary in apparent body stiffness and undulatory wave characteristics, with bluegill sunfish possessing relatively stiff bodies and longer undulatory wavelengths relative to the more flexible and shorter wavelengths displayed by clown knifefish. For the three individuals of each species studied, mean fish total length (L) was 19.7 cm for bluegill and 19.3 cm for knifefish. Experiments were conducted under an approved animal IACUC protocol from Harvard University (#20-03).

Individuals of both species swam in a recirculating flow tank as in previous experiments (Lauder and Drucker, 2004; Lauder, 2006; Lauder and Tytell, 2006) at three speeds: 0.5, 1.0, and 1.5 L/sec. Fish acclimated to the flow tank for several hours before testing began. Two Photron PCI-1024 high-speed cameras taking video at 500 Hz (1 megapixel resolution per

frame) provided side and bottom views of fish undulatory locomotion simultaneously, allowing the calculation of tailbeat frequencies, body curvatures, and Strouhal numbers. We used a custom MATLAB (v7.1, MathWorks, Inc., Natick, MA, USA) program to digitize the midline in images from a ventral view at successive time intervals for both swimming fishes and flexible foils, and another custom program to calculate curvature data from the digitized ventral midline coordinates (also see curvature calculation methods in our previous papers, e.g., Chadwell et al., 2012; Flammang et al., 2013; Standen and Lauder, 2005). We divided the length of each fish and foil into 200 equally spaced points, and calculated the curvature between each set of 16 points using the two end points. This results in the curvature of every 0.5 or 1.0 cm length of the ventral midline depending on the fish or foil length. The maximum curvature was simply the largest curvature value along the length of the body.

Reynolds number is calculated as $(U*L)/\nu$, where U is swimming speed, L is either fish or foil length, and ν is the kinematic viscosity of water (taken as $1.004 * 10^{-6}$ m^2/s at 20° C). Strouhal number equals $(f*A)/U$ where f is the tail beat or flapping frequency, A is the total peak-to-peak tail beat amplitude, and U is swimming speed. Propulsive efficiency is the thrust coefficient divided by the power coefficient (Read et al., 2003), and work is calculated as the force in the y-direction (since the foils were moved in heave (y) only) times the distance moved (we obtain this from motor encoders that measure foil shaft motion). Power is force times velocity of the heave motion, and the power divided by the swimming velocity gives the cost of transport in Joules/meter. The same foil shaft was used to hold all foils and we used the same configuration as in our previous papers using flexible foils (e.g., Alben et al., 2012; Quinn et al., 2014; Wen and Lauder, 2013) in which the shaft holds the foil leading edge between two halves which are screwed together to prevent slipping and bending of the foil leading edge, with the shaft attached to a carriage placed above a recirculating flow tank. We have not "subtracted" the effect of the foil shafts as the test conditions were the same for all foils. Separate tests (not included in this paper) show that the foil shafts do not contribute significantly to thrust because the foils and shafts are moved in heave (side to side motion) only. However, the flat foil shaft holders will increase the recorded y-forces, and hence the calculated cost of transport. The cost of transport data presented here should thus be viewed as comparative among the foils studied, but not directly comparable to data obtained, for example, from metabolic studies of swimming fishes.

For comparison to patterns of fish locomotion, we used two flexible plastic foil materials of two different lengths. The plastic foil material comes from a collection of plastic

453 shim stock (ARTUS Corp., Englewood, NJ) with each thickness coded with a unique color.
454 For convenience of description, we will refer to the two foils used here by their colors and/or
455 stiffnesses: the relatively flexible tan foil material (thickness 0.25 mm) and the relatively stiff
456 yellow foil (thickness 0.5 mm). Foil height is 6.8 cm (chosen to correspond to our previous
457 work with both rigid and flexible foils) with measured flexural stiffnesses of $3.3 * 10^{-5}$ N m^2
458 for tan foils, and $9.9 * 10^{-4}$ N m^2 for yellow foils (see Alben et al., 2012; Lauder et al. 2007,
459 2011a, b). Foil lengths are 10 cm and 20 cm, with masses of 1.0 g and 2.0 g for the flexible
460 tan foils at these respective lengths, and 4.8g and 9.4 g for the stiffer yellow foils.
461 We collected flapping foil data using the mechanical flapping apparatus from our
462 previous research (Alben et al., 2012; Flammang et al., 2011; Lauder et al., 2011a, b, 2012;
463 Quinn et al., 2014; Wen and Lauder, 2013), and we made three general types of
464 measurements on each foil.
465 First, we quantified a "performance surface" for each foil shape and stiffness by
466 varying heave amplitude and frequency: 52 data points served as a map of the performance
467 surface (efficiency or thrust coefficient vs. frequency and heave) with frequency ranging
468 from 0.50 to 3.00 Hz in 0.25 Hz increments, and heave amplitude varying from 1.0 to 3.0 cm
469 in 0.5 cm increments. An ATI Nano-17 six-axis force/torque sensor (ATI Inc., Apex, North
470 Carolina) attached to the foil shaft allowed 3 force and 3 torque measurements in an XYZ
471 coordinate system: X pointed upstream, Z pointed up the shaft, and Y pointed in the
472 direction of heave (normal to the free-stream flow). Foils under these test conditions were
473 anchored above the flow tank with the foil shaft fixed to the heave and pitch motors (see
474 Alben et al., 2012; Quinn et al., 2014; Wen and Lauder, 2013). Flow speeds varied from 0.1
475 to 0.3 m/s. For each performance surface for each foil, and we altered flow speed with heave
476 amplitude so that the Strouhal number for a given frequency remained constant over the
477 heave range. The Strouhal number for each test is equal to 1/5 of the frequency at each
478 different heave value. We replicated each surface five times for each foil, and calculated
479 thrust coefficients and efficiency for each combination of heave and frequency following the
480 equations in Read et al. (2003). Propulsive efficiency equals the thrust coefficient divided by
481 the power coefficient, and work is given as the force in the y-direction (since the foils were
482 moved in heave (y) only) times the distance moved (obtained from motor encoders that
483 measure foil shaft motion). Power is calculated as force times the velocity of heave motion,
484 and power divided by the swimming velocity gives the cost of transport in Joules/meter. The
485 self-propelled speed for each foil on each performance surface (and in the plots shown

beneath in Figures 6 and 7) occurs where the mean thrust coefficient shown on the y-axis (which is averaged over the flapping cycles) is zero.

Because these performance surfaces are hard to visualize in two dimensions in in Figures 6 and 7, we provide as supplemental data two MATLAB .fig files with the data and surfaces for the four foils together: S1.Thrust.surface.fig, and S2.Efficiency.surface.fig. These files can be opened with MATLAB and rotated in three-dimensions to visualize the differences among the swimming flexible foils.

Second, we conducted focused experiments on foils swimming at their self-propelled speed for each foil type at each of the four frequencies. Fish swimming steadily do so at a self-propelled speed where thrust and drag forces are balanced over a tail beat cycle, and it is important to quantify foil swimming performance at self-propelled swimming speeds for comparison to fish data. A LABVIEW program controlling a motor on the carriage moved the shaft with a +/- 1cm sinusoidal heave motion at 0.5, 1, 2, and 3 Hz. We chose these parameters because they closely approximate the heave motion of the mid-body region and the frequencies used by fishes during undulatory propulsion.

Linear and rotary encoders placed on the carriage and the flow motor allowed a second LABVIEW program to calculate the self-propelled speed (SPS) for a foil after trials at a range of flow speeds. For these self-propelled experiments, we attached the foil shaft above the flow tank to linear air-bearings which allowed the foil to "swim" and move along the length of the tank. As foil actuation occurs, foils swim forward as they generate thrust and produce a small restoring force, and flow speed is then tuned to increase drag and bring each foil back to its mean starting position. Foils are thus free to move upstream and downstream over a short distance as the heave motion produces an undulatory wave along the flexible foil. The mean SPS was calculated 3 times for each foil and the results were averaged. This procedure followed our previous research in which flexible foils are allowed to self-propel, and thrust and drag forces are naturally balanced over a flapping cycle (Lauder et al., 2007, 2011a, b, 2012).

Third, flow visualization around swimming foils quantified hydrodynamic patterns at the self-propelled speed for each foil with simultaneous measurement of swimming forces and torques using the ATI Nano-17 force/torque sensor. For these experiments, the foil shafts again were anchored above the flow tank, and the flow speed set to the previously-determined self-propelled speed. Two Photron high-speed cameras captured synchronized lateral and ventral views of the flapping foils. A LABVIEW trigger pulse synchronized the 500 Hz data collection of heave position, force and torque magnitudes, and video frames.

When foils are self-propelling the mean thrust coefficient over a single flapping cycle should equal zero (Lauder et al., 2011a), and this condition was achieved for our self-propelling foils.

For hydrodynamic visualization, a continuous 10W Coherent argon-ion laser light sheet was generated at the mid-foil level, and provided data on the flow patterns generated along the length of the foil and in the wake. Analysis using DaVis 7.2 (LaVision Inc., Goettingen, Germany) particle image velocimetry software as in our previous research (Drucker and Lauder, 2005; Nauen and Lauder, 2002a, b; Esposito et al., 2012) provided velocity vectors describing the flow patterns generated by the self-propelling flexible foils. Using LabChart 7 (ADInstruments, Inc., Colorado Springs, Colorado) software, a low pass filter was applied for Y and Z forces and X and Z torques. A band-pass filter was used for X forces and Y torques to reduce interference from the imposed heave frequency, and filter cutoffs were adjusted appropriately as heave frequency was changed among experiments. Five replicates of separate trials of the 20 cm long tan (flexible) foil actuated at 2 Hz showed a Y force standard error of 0.4% of the mean range and an X force standard error of 1.0% of the mean range. Similar values were obtained for the torques measured.

We performed statistical analyses using JMP Pro version 11 (SAS Inc., Cary North Carolina). Regressions of foil and fish swimming data used frequency as the independent variable and self-propelled speed as the dependent variable. Slopes, intercepts, error estimates for these parameters, and 95% confidence limits are calculated for each fish species and foil type (see Table 1). An analysis of covariance (ANCOVA) provided comparison among regression lines.

ACKNOWLEDGEMENTS

We thank members of the Lauder and Tangorra Labs for many helpful discussions on fish fins and flexible flapping foil propulsion, Silas Alben for assistance in interpreting flapping foil results, Erik Anderson, Vern Baker, and Chuck Witt for their efforts in designing the robotic flapper and control and analysis software, and Grace Xiong for helping collect fish data. Brooke Flammang, Erik Anderson, and Erin Blevins provided many helpful comments on the manuscript.

FUNDING

This work was supported by NSF grants EFRI-0938043 and CDI 0941674 to G. L..

REFERENCES

Affleck, R. J. (1950). Some points in the function, development, and evolution of the tail in fishes. *Proc. Zool. Soc. Lond.* **120**, 349-368.

Alben, S., Baker, T. V., Witt, C., Anderson, E. J. and Lauder, G. V. (2012). Dynamics of freely swimming flexible foils. *Phys. Fluids A*, **24**, 051901.

Bainbridge, R. (1958). The speed of swimming of fish as related to size and to the frequency and amplitude of the tail beat. *J. Exp. Biol.* **35**, 109-133.

Barrett, D. S., Triantafyllou, M. S., Yue, D. K. P., Grosenbaugh, M. A. and Wolfgang, M. J. (1999). Drag reduction in fish-like locomotion. *J. Fluid Mech.* **392,** 183-212.

Beal, D. N., Hover, F. S., Triantafyllou, M. S., Liao, J. and Lauder, G. V. (2006). Passive propulsion in vortex wakes. *J. Fluid Mech.* **549**, 385-402.

Bhalla, A. P. S., Griffith, B. E. and Patankar, N. A. (2013). A forced damped oscillation framework for undulatory swimming provides new insights into how propulsion arises in active and passive swimming. *PLoS Comput Biol* **9**, e1003097.

Borazjani, I., Sotiropoulos, F., Tytell, E.D . and Lauder, G. V. (2012). On the hydrodynamics of the bluegill sunfish c-start escape response: three-dimensional simulations and comparison with experimental data. *J. Exp. Biol.* **215**, 671-684.

Chadwell, B. A., Standen, E. M., Lauder, G. V. and Ashley-Ross, M. A. (2012). Median fin function during the escape response of bluegill sunfish (*Lepomis macrochirus*). II: fin-ray curvature. *J. Exp. Biol.* **215**, 2881-2890.

Donley, J. and Dickson, K. A. (2000). Swimming kinematics of juvenile Kawakawa tuna (*Euthynnus affinis*) and chub mackerel (S*comber japonicus*). *J. Exp. Biol.* **203**, 3103-3116.

Drucker, E. G. and Lauder, G. V. (2000). A hydrodynamic analysis of fish swimming speed: wake structure and locomotor force in slow and fast labriform swimmers. *J. Exp. Biol.* **203**, 2379-2393.

Drucker, E. G. and Lauder, G. V. (2005). Locomotor function of the dorsal fin in rainbow trout: kinematic patterns and hydrodynamic forces. *J. Exp. Biol.* **208**, 4479-4494.

Esposito, C., Tangorra, J., Flammang, B. E. and Lauder, G. V. (2012). A robotic fish caudal fin: effects of stiffness and motor program on locomotor performance. *J. Exp. Biol.* **215**, 56-67.

Flammang, B. E., Lauder, G. V., Troolin, D. R. and Strand, T. (2011). Volumetric imaging of shark tail hydrodynamics reveals a three-dimensional dual-ring vortex wake structure. *Proc. Royal Soc. B* **278**, 3670-3678.

Flammang, B. E., Alben, S., Madden, P. G. A. and Lauder, G. V. (2013). Functional morphology of the fin rays of teleost fishes. *J. Morphol.* **274**, 1044–1059.

Gibb, A.C., Dickson, K.A., Lauder, G.V. (1999). Tail kinematics of the chub mackerel Scomber japonicus: testing the homocercal tail model of fish propulsion. *J. Exp. Biol.* **202**: 2433-47

Hua, R.-N., Zhu, L. and Lu, X.-Y. (2013). Locomotion of a flapping flexible plate. *Phys. Fluids* **25**, 121901.

Jayne, B.C. and Lauder, G.V. (1993). Red and white muscle activity and kinematics of the escape response of the bluegill sunfish during swimming. *J Comp Physiol A* **173**, 495-508.

Jayne, B. C. and Lauder, G. V. (1994). How swimming fish use slow and fast muscle fibers: implications for models of vertebrate muscle recruitment. *J. Comp Physiol A* **175**, 123-131.

Jayne, B. C. and Lauder, G. V. (1995a) Speed effects on midline kinematics during steady undulatory swimming of largemouth bass, *Micropterus salmoides. J. Exp. Biol.* **198**, 585-602.

Jayne, B. C. and Lauder, G. V. (1995b). Red muscle motor patterns during steady swimming in largemouth bass: effects of speed and correlations with axial kinematics. *J. Exp. Biol.* **198**, 1575-1587.

Jayne, B. C. and Lauder, G. V. (1995c). Are muscle fibers within fish myotomes activated synchronously? Patterns of recruitment within deep myomeric musculature during swimming in largemouth bass. *J. Exp. Biol.* **198**, 805-815.

Johnson, T .P., Syme, D. A., Jayne, B. C., Lauder, G. V. and Bennett, A. F. (1994). Modeling red muscle power output during steady and unsteady swimming in largemouth bass (*Micropterus salmoides*). *Am. J. Physiol.* **267**, R481-R488.

Katz, J. and Weihs, D. (1979). Large amplitude unsteady motion of a flexible slender propulsor. *J. Fluid Mech.* **90**, 713-723.

Lauder, G. V. and Drucker, E. G. (2004). Morphology and experimental hydrodynamics of fish fin control surfaces. *IEEE J. Ocean. Eng.* **29**, 556-71.

Lauder, G. V. (2006). Locomotion, In *The Physiology of Fishes, Third Edition*, ed D H Evans and J B Claiborne (Boca Raton: CRC Press) pp 3-46.

Lauder, G. V. and Tytell, E. D. (2006). Hydrodynamics of undulatory propulsion, In *Fish Biomechanics. Volume 23 in Fish Physiology*, ed R E Shadwick and G V Lauder (San Diego: Academic Press) pp 425-68

Lauder, G. V., Anderson, E. J., Tangorra, J. and Madden, P. G. A. (2007). Fish biorobotics: kinematics and hydrodynamics of self-propulsion. *J. Exp. Biol.* **210**, 2767-2780.

Lauder, G., Tangorra, J., Lim, J., Shelton, R., Witt, C. and Anderson, E. J. (2011a). Robotic models for studying undulatory locomotion in fishes. *Marine Tech. Soc. J.* **45**, 41-55.

Lauder, G. V., Madden, P. G. A., Tangorra, J., Anderson, E. and Baker, T. V. (2011b). Bioinspiration from fish for smart material design and function. *Smart Mater. Struct.* **20:**doi:10.1088/0964-1726/20/9/094014.

Lauder, G. V., Flammang, B. E. and Alben, S. (2012). Passive robotic models of propulsion by the bodies and caudal fins of fish. *Int. Comp. Biol.* **52**, 576–587.

Liao, J., Beal, D. N., Lauder, G. V. and Triantafyllou, M. S. (2003a). Fish exploiting vortices decrease muscle activity. *Science* **302**, 1566-1569.

Liao, J., Beal, D. N., Lauder, G. V. and Triantafyllou, M. S. (2003b). The Kármán gait: novel body kinematics of rainbow trout swimming in a vortex street. *J. Exp. Biol.* **206**, 1059-1073.

Liao, J. (2004). Neuromuscular control of trout swimming in a vortex street: implications for energy economy during the Karman gait. *J. Exp. Biol.* **207**, 3495-3506.

Liu, J.-D. and Hu, H. (2006). Biologically inspired behaviour design for autonomous robotic fish. *Internat. J. Automat. Comput.* **3**, 336-347.

Long, J. H., McHenry, M. J. and Boetticher, N. C. (1994). Undulatory swimming: how traveling waves are produced and modulated in sunfish (*Lepomis gibbosus*). *J. Exp. Biol.* **192**, 129-145.

Long, J. (1998). Muscles, elastic energy, and the dynamics of body stiffness in swimming eels. *Amer. Zool.* **38**, 771-792.

Long, J., Koob-Emunds, M., Sinwell, B. and Koob, T. J. (2002). The notochord of hagfish *Myxine glutinosa*: visco-elastic properties and mechanical functions during steady swimming. *J. Exp. Biol.* **205:**3819-3831.

Long, J. H., Schumacher, J., Livingston, N. and Kemp, M. (2006a). Four flippers or two? Tetrapodal swimming with an aquatic robot. *Bioinsp. Biomimet.* **1**, 20-29.

Long, J., Koob, T., Irving, K., Combie, K., Engel, V., Livingston, N., Lammert, A. and Schumacher, J. (2006b). Biomimetic evolutionary analysis: testing the adaptive value of vertebrate tail stiffness in autonomous swimming robots. *J. Exp. Biol.* **209**, 4732-4746.

Long, J.H., Krenitsky, N.M., Roberts, S.F., Hirokawa, J., de Leeuw, J. and Porter, M.E. (2011). Testing biomimetic structures in bioinspired robots: how vertebrae control the stiffness of the body and the behavior of fish-like swimmers. *Int. Comp. Biol.* **51**, 158-175.

Magnuson, J. J. (1978). Locomotion by scombrid fishes: hydromechanics, morphology, and behavior. In Fish Physiology. Vol. VII. Locomotion, (W. S. Hoar and D. J. Randall, eds.), pp. 239-313. New York: Academic Press.

McHenry, M. J., Pell, C. A. and Long, J. A. (1995). Mechanical control of swimming speed: stiffness and axial wave form in undulating fish models *J. Exp. Biol.* **198**, 2293-2305.

Nauen, J. C. and Lauder, G. V. (2002a). Hydrodynamics of caudal fin locomotion by chub mackerel, *Scomber japonicus* (Scombridae). *J. Exp. Biol.* **205**, 1709-1724.

Nauen, J. C. and Lauder, G. V. (2002b). Quantification of the wake of rainbow trout (*Oncorhynchus mykiss*) using three-dimensional stereoscopic digital particle image velocimetry. *J. Exp. Biol.* **205**, 3271-3279.

Quinn, D. B., Lauder, G. V. and Smits, A. J. (2014). Scaling the propulsive performance of heaving flexible panels. J. Fluid Mech. **738**, 250-267.

Peng, J., Dabiri, J. O., Madden, P. G. and Lauder, G. V. (2007). Non-invasive measurement of instantaneous forces during aquatic locomotion: a case study of the bluegill sunfish pectoral fin. *J. Exp. Biol.* **210**, 685-698.

Peng, J. and Dabiri, D. (2008). An overview of a Lagrangian method for analysis of animal wake dynamics. *J. Exp. Biol.* **211**, 280-287.

Ramananarivo, S., Godoy-Diana, R. and Thiria, B. (2013). Passive elastic mechanism to mimic fish-muscle action in anguilliform swimming. *J. Roy. Soc. Interface* **10**, 20130667.

Read, D. A., Hover, F. S. and Triantafyllou, M. S. (2003). Forces on oscillating foils for propulsion and maneuvering. *J. Fluids Struct.* **17**, 163-183.

Rome, L. C., Swank, D. and Corda, D. (1993). How fish power swimming *Science* **261:**340-343.

Standen, E. M. and Lauder, G. V. (2005). Dorsal and anal fin function in bluegill sunfish *Lepomis macrochirus*: three-dimensional kinematics during propulsion and maneuvering. *J. Exp. Biol.* **208**, 2753-2763.

Syme, D. A. and Shadwick, R. (2002). Effects of longitudinal body position and swimming speed on mechanical power of deep red muscle from skipjack tuna (*Katsuwonus pelamis*). *J. Exp. Biol.* **205**, 189-200.

Tangorra, J. L., Lauder, G. V., Hunter, I. W., Mittal, R., Madden, P. G. A. and Bozkurttas, M. (2010). The effect of fin ray flexural rigidity on the propulsive forces generated by a biorobotic fish pectoral fin. *J. Exp. Biol.* **213**, 4043-4054.

Tytell, E.D. (2004). Kinematics and hydrodynamics of linear acceleration in eels, *Anguilla rostrata*. *Proc. Roy. Soc. Lond. B* **271**, 2535-2540.

Tytell, E. D. (2006). Median fin function in bluegill sunfish Lepomis macrochirus: streamwise vortex structure during steady swimming. *J. Exp. Biol.* **209**, 1516-1534.

Tytell, E.D. and Lauder, G.V. (2008). Hydrodynamics of the escape response in bluegill sunfish, Lepomis macrochirus. *J. Exp. Biol.* **211**, 3359-3369.

Tytell, E. D., Standen, E. M. and Lauder, G. V. (2008). Escaping Flatland: three-dimensional kinematics and hydrodynamics of median fins in fishes. *J. Exp. Biol.* **211**, 187-195.

Webb, P. W. (1975). Hydrodynamics and energetics of fish propulsion. *Bull. Fish Res. Bd. Can.* **190**, 1-159.

Webb, P. (2006). Stability and maneuverability, In *Fish Biomechanics. Volume 23 in Fish Physiology*, ed R E Shadwick and G V Lauder (San Diego: Academic Press) pp 281-332.

Wen, L. and Lauder, G. V. (2013). Understanding undulatory locomotion in fishes using an inertia-compensated flapping foil robotic device. *Bioinsp. Biomimet.* **8**, 046013.

Table

Table 1. Linear regression equation parameters and the statistical fit for each foil type and each fish species plotted in Figure 3. Regressions are calculated from all raw data points. ANCOVA results comparing regressions are given in the text.

	Slope (s.e.)	Intercept (s.e.)	R^2	Model F-value (df)	P-value
Tan 10	8.6 (0.4)	2.3 (0.7)	0.98	571 (11)	<.001
Tan 20	8.9 (0.2)	0.75 (0.3)	0.99	2772 (11)	<.001
Yellow 10	10.7 (0.6)	1.2 (1.1)	0.97	310 (11)	<.001
Yellow 20	11.4 (0.9)	-0.19 (1.7)	0.94	162 (11)	<.001
Bluegill	9.0 (1.8)	3.1 (5.4)	0.78	24 (8)	<.001
Knifefish	9.9 (0.6)	-1.9 (1.2)	0.98	304 (11)	<.001

df = regression degrees of freedom; s.e. = standard error of estimate

Figure captions

Fig. 1. Kinematics of swimming fishes. (a), (b) Ventral images of a clown knifefish swimming at 23 $cm \cdot s^{-1}$ and bluegill sunfish swimming 39 $cm \cdot s^{-1}$ respectively when the tail tips are at their maximum amplitude. (c), (d) Ventral midlines of the above fish species digitized from high-speed videos, with two additional images from intermediate states to display the change in shape of the entire fish body over one tail beat cycle. The outlines represent the body midines at four equally-spaces times within a single tail beat cycle. (e), (f) Zoomed-in midlines showing the posterior body shape over one tail beat cycle. Dashed lines indicate the expanded portion of the fish body waveform shown in the two bottom panels. The waveform profiles for these fish closely resemble the shapes formed from flapping foils under certain motion programs (see Fig. 2).

Fig. 2. The Tan 10 cm, Tan 20 cm (flexural stiffness = $3.3 * 10^{-5}$ $N*m^2$), Yellow 10 cm, and Yellow 20 cm (flexural stiffness = $9.9 * 10^{-4}$ $N*m^2$) plastic foils actuated at the leading edge with an amplitude of +/- 1.0 cm heave at 0.5, 1.0, 2.0, and 3.0 Hz while swimming at self-propelled speed and being filmed from below. For each variable condition, one heave cycle is shown depicted by four evenly spaced midlines. The number of visible waves increases as foil length, flexibility, and frequency increase. Note the overall similarities in waveform between the Yellow 10 cm foil moving at 2 Hz, and the bluegill body shapes (Fig. 1f), and the Tan 10 cm long foil moving at 2 Hz, and knifefish body shapes (Fig. 1e).

Fig. 3. Self-propelled speed plotted versus cycle frequency for the different foils and fishes. Each point represents a mean with error bars equal to two standard errors. Some error bars are hidden behind markers. Regression lines are calculated from entire raw data sets with residuals along the y-axis for foils and the x-axis for fishes. The fish regression lines are similar to the foil lines demonstrating that the simple flapping foils are a good model for undulating fish propulsion. Regression statistics are provided in Table 1. ANCOVA analysis demonstrates that the regression lines for the two fish species and both tan foils have similar slopes, while the slopes for the two yellow foils are significantly greater (see text for discussion).

Fig. 4. Maximum measured curvatures along the body of foils and fishes swimming at different frequencies. Stiff yellow foils have lower maximum curvatures than flexible tan

foils and foil length has no impact on maximum curvature. Bluegill sunfish maximum curvatures fall in the range of the robotic foil models, while the clown knifefish curvatures are higher than the foil models. These data do not include the high curvatures seen at the very tip of the flexible knifefish tail (figure 1c).

Fig. 5. Plots of measured variables from swimming fishes and flexible foils to show how these variables change with increasing frequency. Error bars are not shown as they would be contained within the symbols (see Materials and Methods for further error estimates). (a), (b) Reynolds and Strouhal numbers showing similarities between robotic flapping foils and fishes. (c), (d), (e) Force and torque ranges measured over 4 seconds oriented with X upstream, Y in the direction of heave, and Z up the shaft. Yellow foils (flexural stiffness = $9.9 * 10^{-4}$ N*m^2) produce higher force and torque ranges than tan foils ($3.3 * 10^{-5}$ N*m^2). (f), (g), (h) Work and cost of transport graphs show yellow foils require more work and energy per meter to swim but less energy relative to the mass of the foils. Foil length has little impact on force, torque, and work, but short foils have lower cost of transport relative to mass.

Fig. 6. Locomotor performance of 10 cm long flexible (tan) and stiff (yellow) foils comparing thrust and efficiency over a range of different heave and frequency motion programs. Thrust coefficient and efficiency are dimensionless. Three-dimensional surfaces in the top panels are available as supplemental MATLAB files (S1.Thrust.surface.fig; S2.Efficiency.surface.fig), and are plotted based on 52 experimental points at different heaves and frequencies. Plots below the performance surfaces illustrated in the top panels are shown for free-stream flow at 0.1, 0.2 and 0.3 m/s. Surfaces and lines are the mean of 5 trials; error bars are one standard error. Plots represent transects through the performance surfaces at different heave values, and efficiency plots show positive efficiencies only. Note that stiff (yellow) foils have higher thrust coefficients than more flexible (tan) foils and that at 0.1 and 0.2 m/s swimming speed there is an efficiency cross-over point where the flexible foil becomes more efficient than the stiff foil. Self-propulsion occurs where the mean thrust coefficient shown on the y-axis (averaged over the flapping cycles) is zero.

Fig. 7. Locomotor performance of 20 cm long flexible (tan) and stiff (yellow) foils comparing thrust and efficiency over a range of different heave and frequency motion programs. Thrust coefficient and efficiency are dimensionless. Three-dimensional surfaces in the top panels are available as supplemental MATLAB files (S1.Thrust.surface.fig; S2.Efficiency.surface.fig),

and are plotted based on 52 experimental points at different heaves and frequencies. Surfaces and lines are the mean of 5 trials; error bars are one standard error. Plots below the performance surfaces illustrated in the top panels are shown for free-stream flow at 0.1, 0.2 and 0.3 m/s. Efficiency plots show positive efficiencies only. Note that stiff 20 cm long yellow foils have higher thrust coefficients than the flexible tan foils and are substantially more efficient at all but the highest frequencies at 0.1 m/s swimming speed. Self-propulsion occurs where the mean thrust coefficient shown on the y-axis (averaged over the flapping cycles) is zero.

Fig. 8. Forces in the x and y-directions and thrust and power coefficients calculated from one cycle of +/- 1cm heave at 2Hz frequency for the four foils swimming at their self-propelled speeds. Error bars of two standard errors for variation among cycles are smaller than the thickness of the lines. (a) Fx curves have two force peaks for each cycle. (b) Fy curves have one peak per cycle and experience forces 10 to 15 times larger than thrust. (c) Thrust coefficients average to zero over a flapping cycle since the foil is self-propelling. (d) Mean power coefficients range from 0.24 to 0.47 for the four foils.

Fig. 9. Hydrodynamic analysis of foil propulsion synchronized with force data for the tan 10 cm foil (left panels, flexural stiffness = $3.3 * 10^{-5}$ $N*m^2$) and the yellow 10 cm foil (right panels, $9.9 * 10^{-4}$ $N*m^2$) at self-propelled speeds (29 cm/s and 32 cm/s respectively) when actuated at the leading edge at 3Hz and amplitude +/- 1cm. (a), (b) Minimum Fx occurs just prior to maximum heave. (c), (d) Maximum Fx occurs just prior to the heave motion reaching its midpoint. A strong leading edge vortex is present in both images enhancing thrust. Fy is force in the direction of heave and has a 17% phase shift from heave for both tan and yellow foils. White lines have been added to mark the ventral foil edge of the foils. Black arrows show the time on the force traces corresponding to each image of flow patterns. Blue (encoder) curves show the heave motion of the foil with +/- 1 cm excursion.

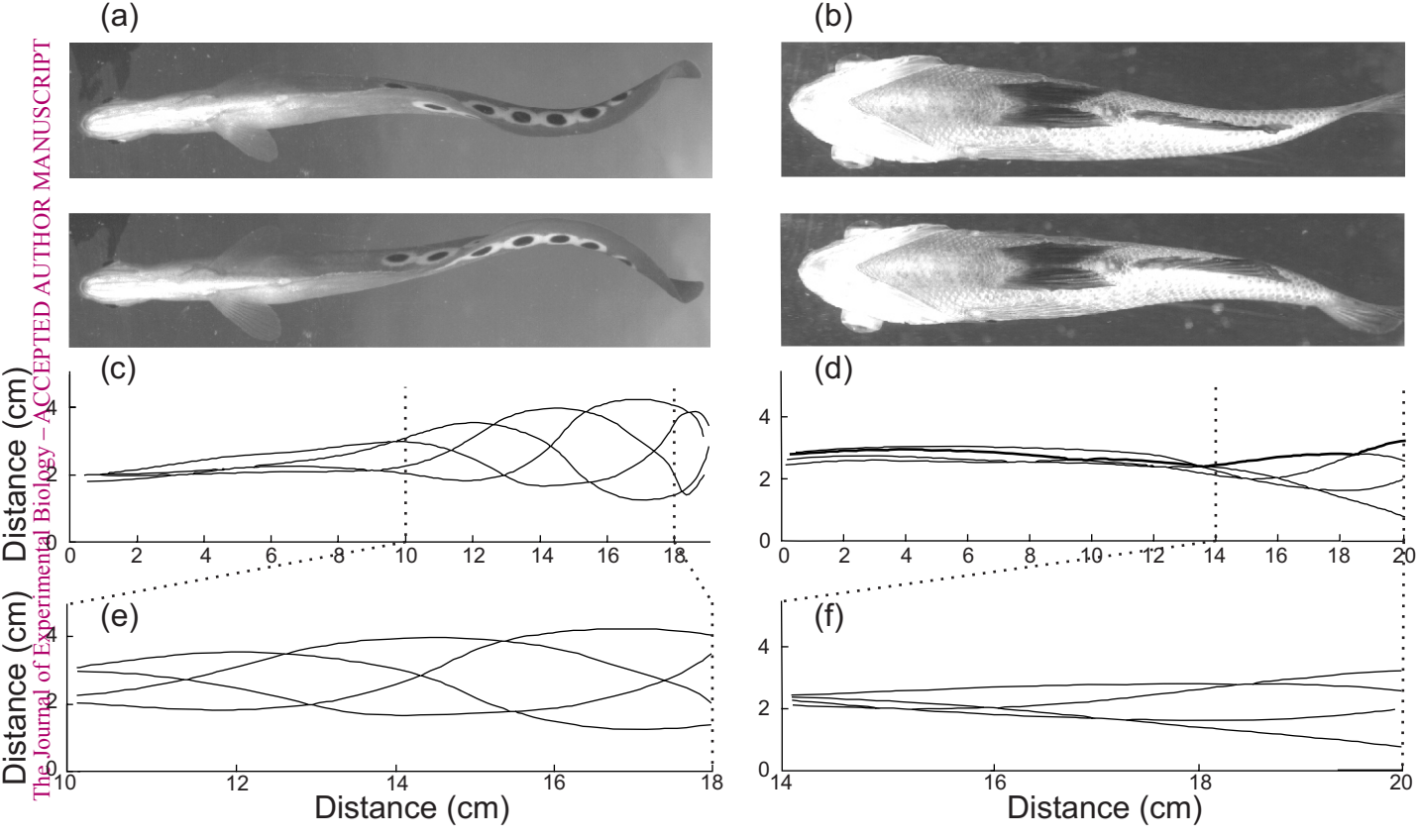

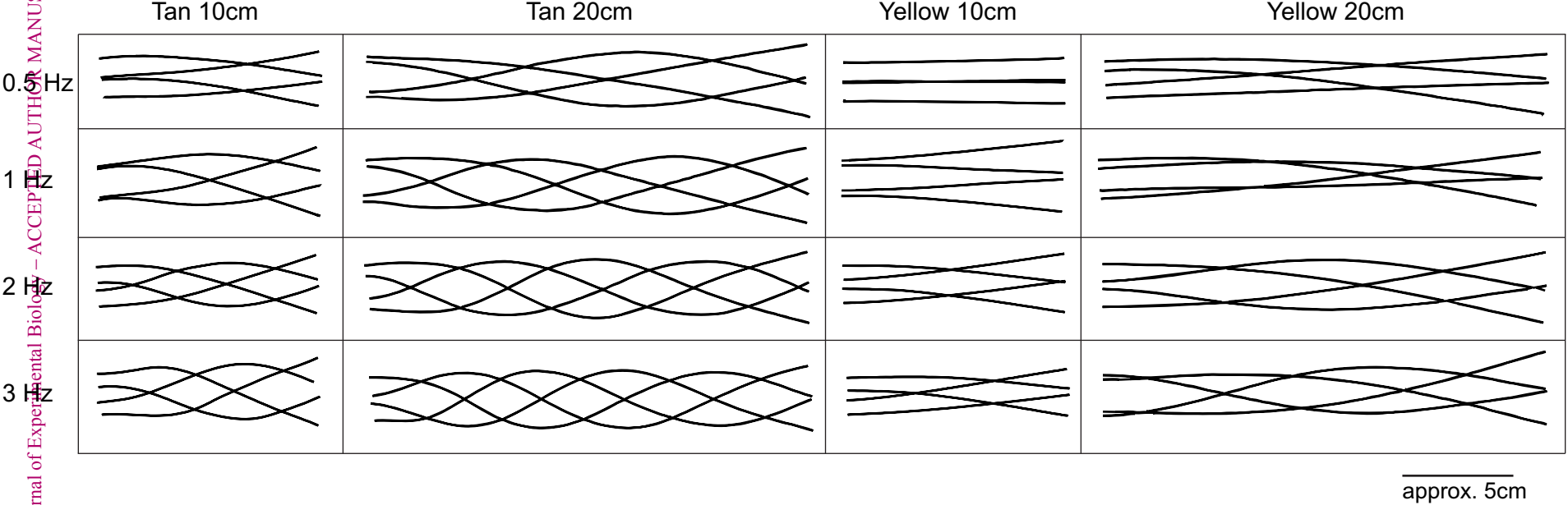

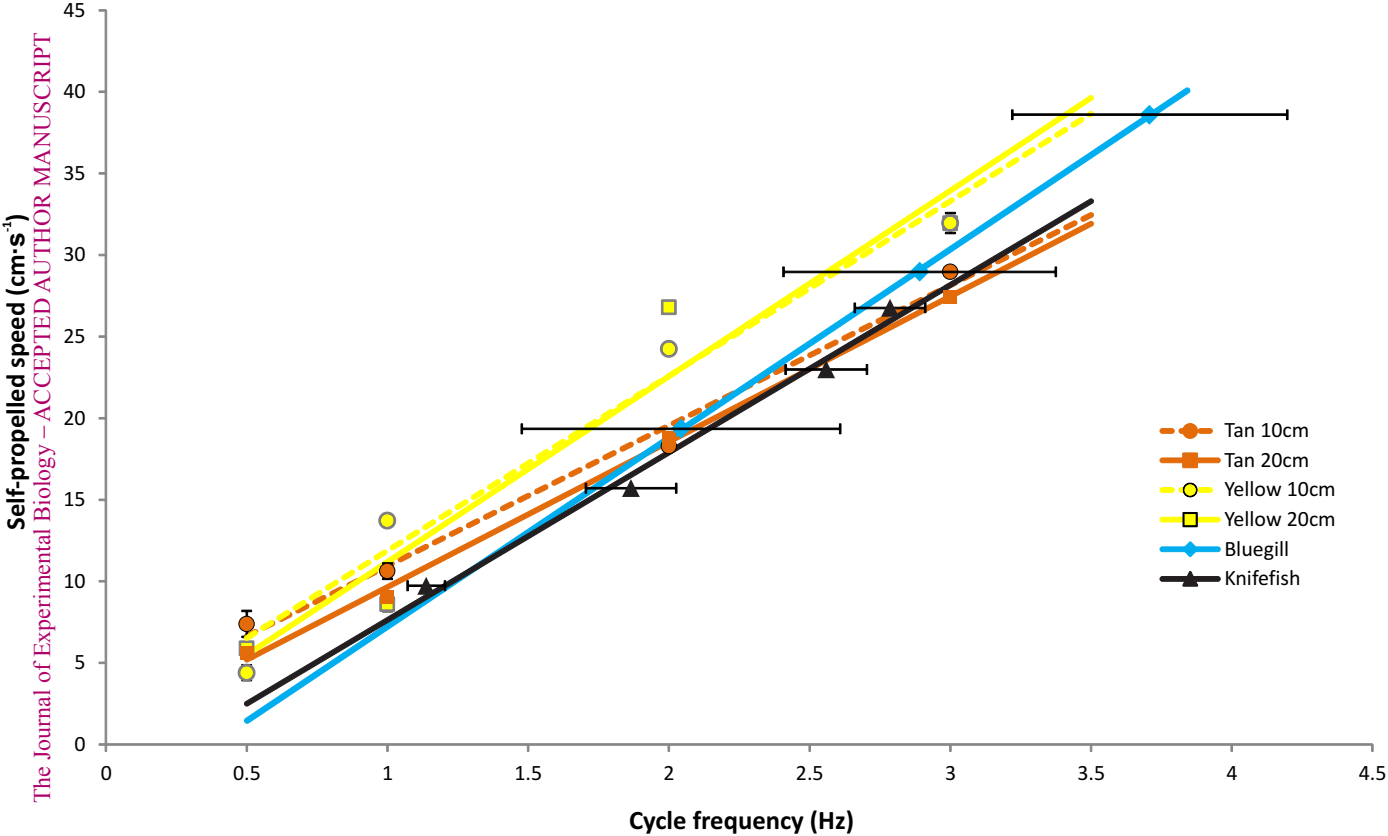

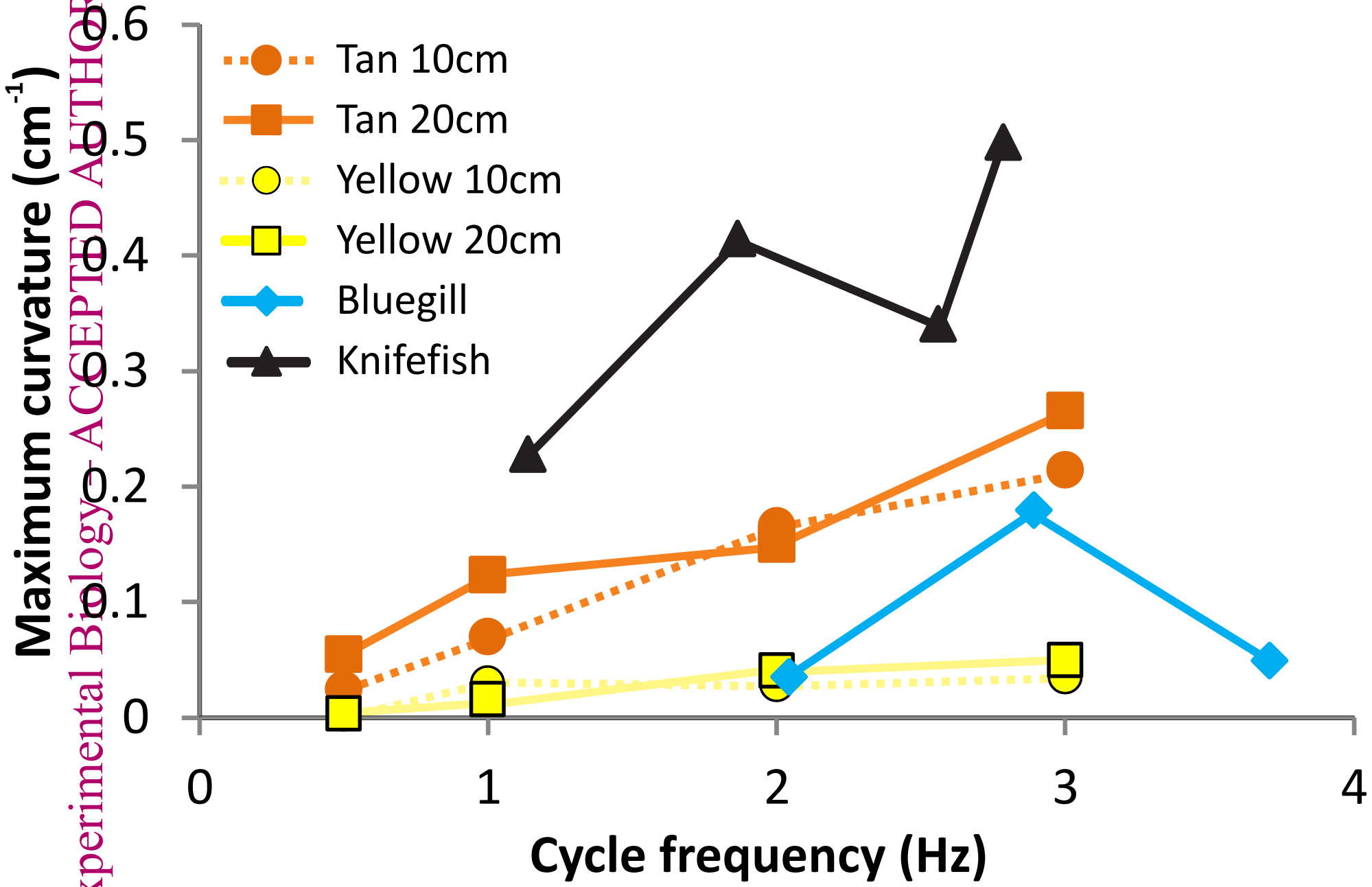

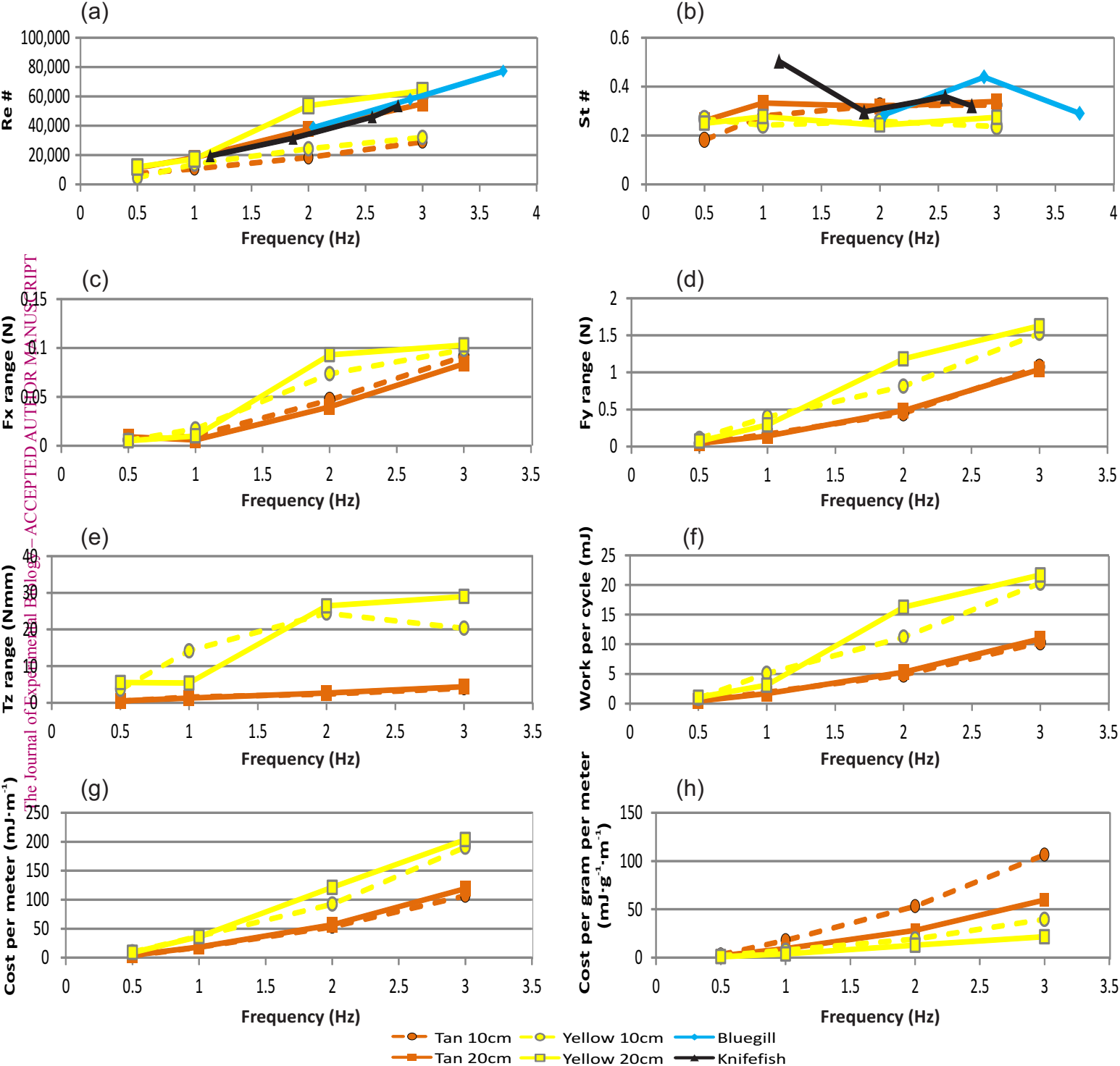

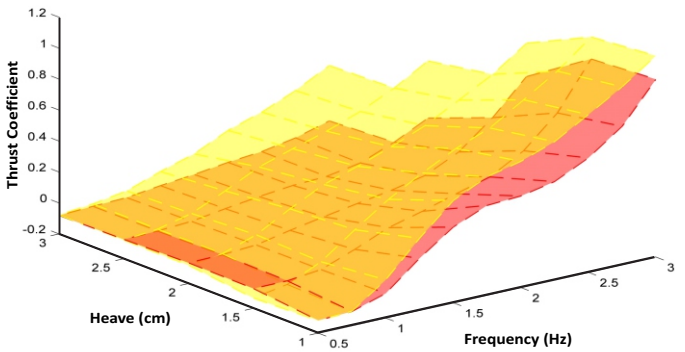

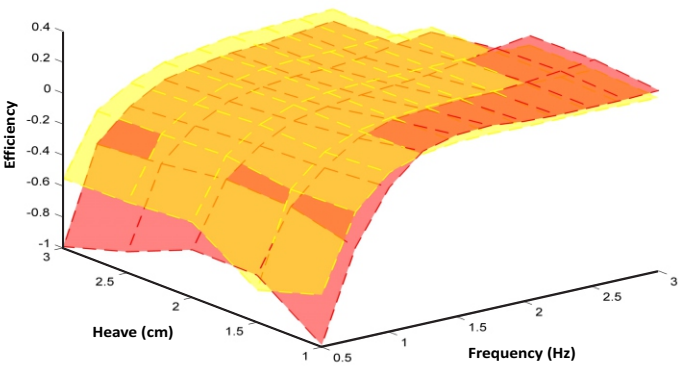

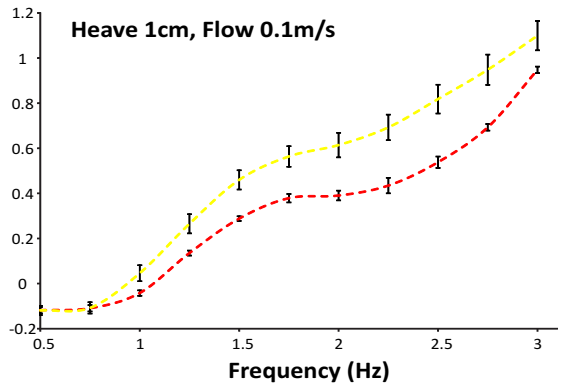

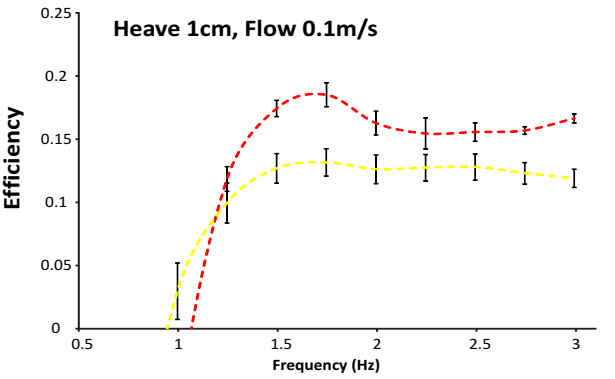

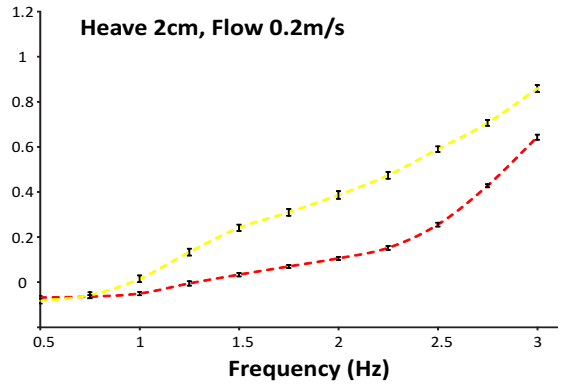

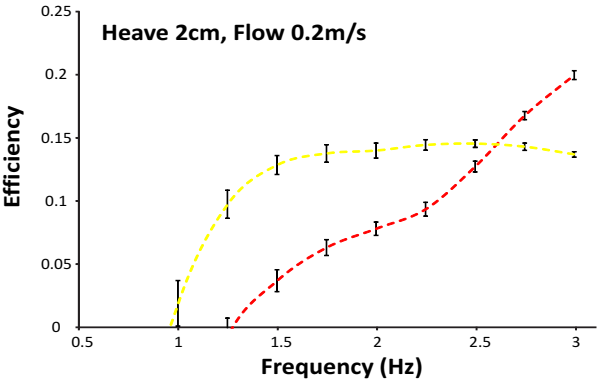

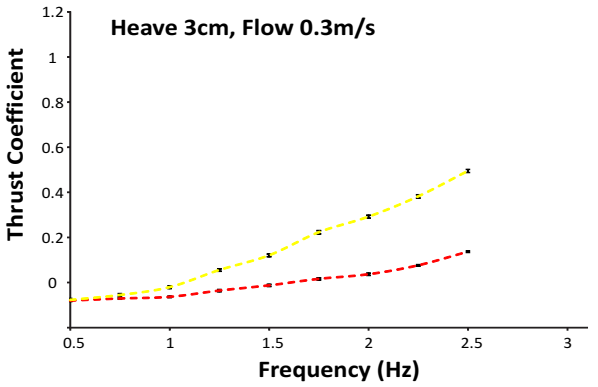

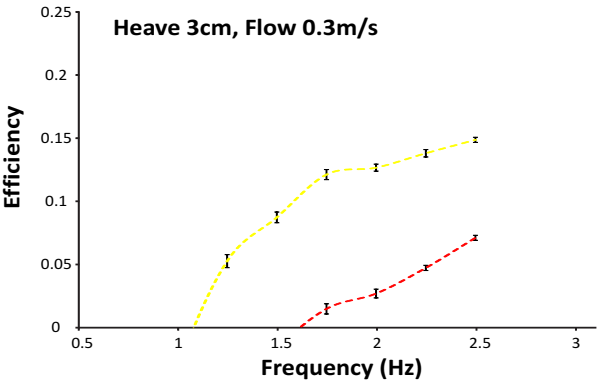

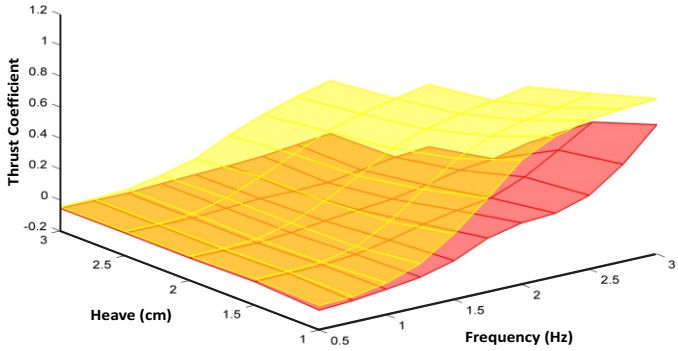

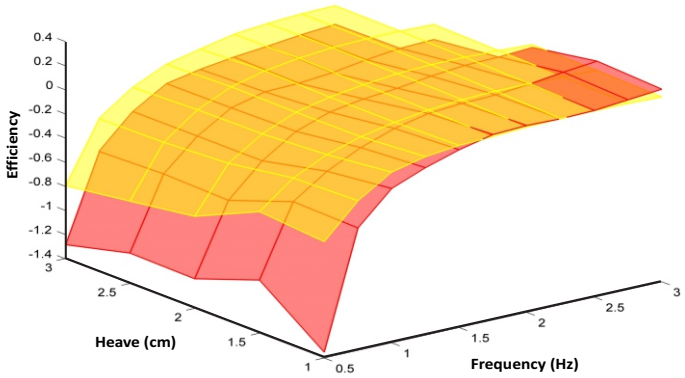

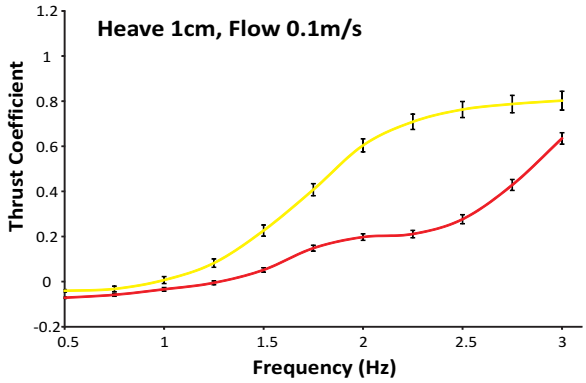

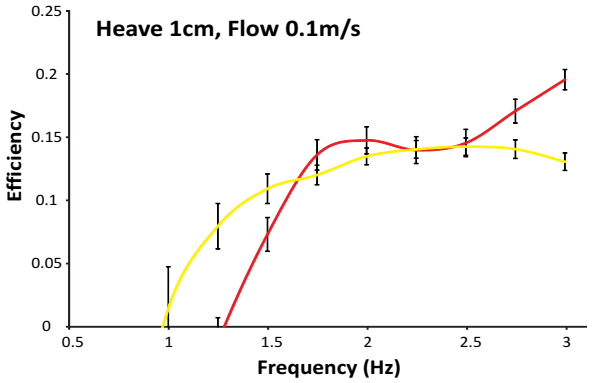

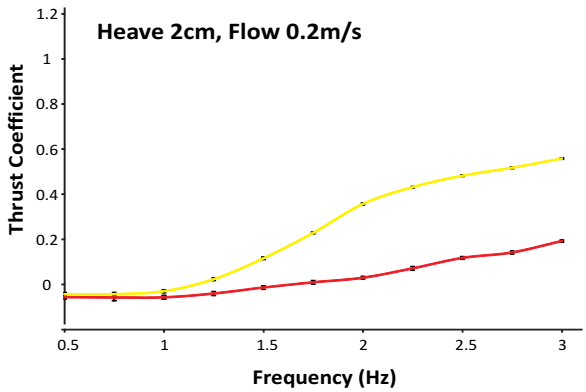

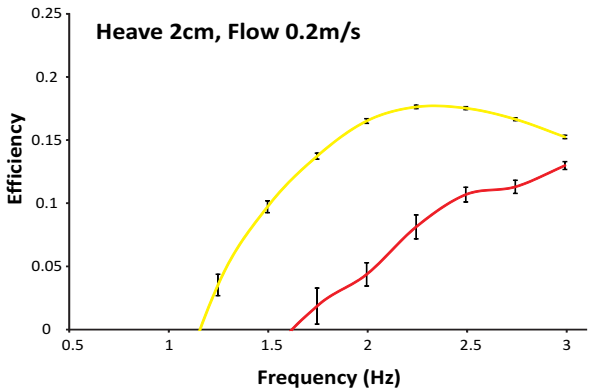

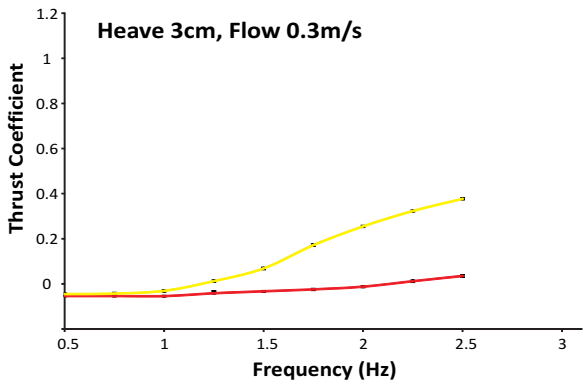

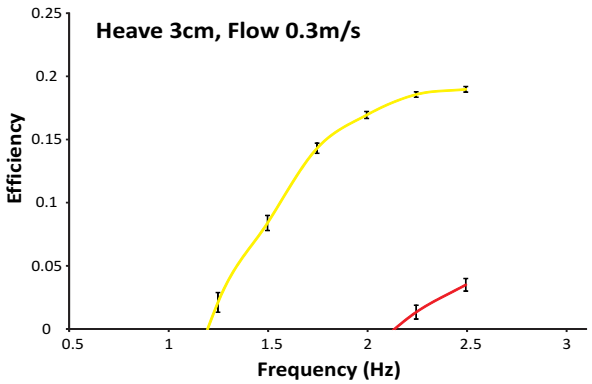

Tan 20cm Yellow 20cm